Theoretical Studies on the Thermodynamics and Kinetics of the N-Glycosidic Bond Cleavage in Deoxythymidine Glycol

Ze-qin Chen,[†,‡] Cheng-hua Zhang,[†] and Ying Xue*[,†]

College of Chemistry, Key Laboratory of Green Chemistry and Technology in Ministry of Education, Sichuan University, Chengdu 610064, and College of Chemistry and Chemical Engineering, China West Normal University, Nanchong 637002, People's Republic of China

Received: April 10, 2009; Revised Manuscript Received: June 10, 2009

The thermodynamic and kinetic properties for the nonenzymatic N-glycosidic bond cleavage in *cis*-(5*R*,6*S*)-5,6-dihydroxy-5,6-dihydrodeoxythymidine (deoxythymidine glycol, dTg) were studied by computational techniques. Optimized structures for all of the stationary points in the gas phase were investigated using the BHandHLYP/6-311++G(d,p) and B3LYP/6-311++G(d,p) methods. Single-point energies were determined employing the ab initio MP2 method in conjunction with the 6-311++G(d,p) basis set. For the unimolecular decomposition of dTg in the gas phase, two pathways were characterized. Subsequently, the hydrolysis of dTg by a single water molecule was investigated. Two possible pathways were considered, involving the abstraction of the C2′ hydrogen followed by the attack of water on the C1′=C2′ bond (S_N1 pathway) and the attack of a water molecule on the C1′ atom with the simultaneous cleavage of the glycosidic bond (S_N2 pathway). However, both the unimolecular decomposition reaction and the hydrolysis reaction involve large energy barriers, suggesting that the role of water is not beneficial to the overall reaction and the direct involvement of a sole water molecule as a nucleophile is unlikely. This result emphasizes the important catalytic role of enzymes. In addition, the solvent effect of water on the four processes was assessed at the geometry optimization level by means of the conductor-like polarized continuum model. Single-point computation was done at the MP2/6-311++G(d,p)//BHandHLYP/6-311++G(d,p) level. The calculated results show that the presence of the solvent water substantially lowers all energy barriers. Our results give out a greater fundamental understanding of the effects of the nucleophile water and solvent water for this important biological reaction.

1. Introduction

Oxidative damage to DNA arises continuously in cells. It is mainly induced by a variety of potentially damaging free radical species (ROS), e.g., $^{\bullet}OH$ and $O_2^{\bullet-}$, which are formed by intracellular respiratory metabolism and extracellular genotoxic agents, such as ultraviolet radiation, ionizing radiation, and chemical species. In many cases, these free radicals attack DNA and produce a variety of lesions, including sugar and base modifications, DNA−protein cross-links, and strand breaks.[1] Studies have shown that oxidative damage to DNA often causes deleterious influences on the cell, including carcinogenesis, mutagenesis, aging, and lethality.[2−4] To hold back these biological injuries to DNA, cells are equipped with repair systems to take care of the different oxidative DNA damage. The major mechanisms involved in the repair processes include base excision as well as nucleotide excision and recombination.

The reaction of thymine base with ROS leads to the formation of thymine glycol (5,6-dihydroxy-5,6-dihydrothymine or Tg),[5] which is also formed by oxidation of 5-methylcytosine followed by hydrolytic deamination of the unstable 5-methylcytosine glycol.[6,7] Tg has been detected in animal and human urine.[8,9] There are four stereoisomers of Tg, i.e., (5*R*,6*S*), (5*R*,6*R*), (5*S*,6*R*), and (5*S*,6*S*) forms, due to the chirality of the C5 and C6 atoms. However, Tg exists in DNA as either the 5*R* *cis*−*trans* pair (5*R*,6*S*; 5*R*,6*R*) or the 5*S* *cis*−*trans* pair (5*S*,6*R*; 5*S*,6*S*) in solution, due to epimerization at the C6 position.[10] Many experiments were devoted in the past two decades to study the stabilities of the four stereoisomers at the nucleoside level or in DNA.[10−14] It has been reported that the 5*R* pair is more abundant and more stable. For the 5*R* and 5*S* pairs, the *cis* epimers predominate at the nucleoside level, the equilibrium ratio being 87% *cis* to 13% *trans* epimers.[10] The oxidation of thymidine or thymidine-containing oligonucleotides preferentially yields the (5*R*,6*S*)-thymidine glycol.[11,12] The same preference [the ratio of the (5*R*,6*S*) and (5*S*,6*R*) isomers was 6:1] was observed in a study on the chemical synthesis of thymine glycol-containing oligonucleotides using a phosphoramidite building block.[13] For the duplex containing the Tg·A pair, the equilibrium ratio of *cis*-(5*R*,6*S*) to *trans*-(5*R*,6*R*) epimers was 7:3 at 30 °C.[14] For a duplex containing the Tg·G pair, the *cis*-(5*R*,6*S*):*trans*-(5*R*,6*R*) equilibrium strongly favored the *cis*-(5*R*,6*S*) epimer; the level of the *trans*-(5*R*,6*R*) epimer remained below the level of detection by NMR.[14] Theoretical investigations have also been undertaken to predict the stability of different isomers of thymine glycol.[14,15] It was found that the *cis*-(5*R*,6*S*) diastereoisomer is the most stable.

The mutation-causing Tg, albeit minor events,[16] effectively inhibits DNA polymerase activities[17,18] and blocks DNA replication,[19] so it must be repaired.[20] It was reported that about 320 Tg sites are repaired by an average human cell every day.[21] Tg is repaired mainly by base excision repair (BER). In *Escherichia coli*, endonuclease III (Nth) and endonuclease VIII (Nei), being

* To whom correspondence should be addressed. E-mail: yxue@scu.edu.cn. Phone: 86-28-85418330.
† Sichuan University.
‡ China West Normal University.

10.1021/jp903334j CCC: $40.75
Published on Web 07/09/2009

bifunctional glycosylases with both glycosylase and lyase activities, can actively excise Tg from DNA through removing the damaged nucleobase by glycosyl transfer using an amine nucleophile from the enzyme,[22,23] and the homologues are well conserved in various organisms.[24−27] Recently, a novel monofunctional Tg-DNA glycosylase activity has been shown to be of the prominent nuclear activities present in some mouse tissues,[28] which repairs disparate types of DNA damage through hydrolyzing the N-glycosidic bonds to create a common product, namely, an abasic site. Biochemical studies on base excision repair revealed that the stereochemistry of Tg is recognized by proteins responsible for these biological processes. Among the base excision repair enzymes for Tg, *E. coli* endonuclease VIII, mouse and human NTH1 (hNTH1), and human NEIL1 (hNEIL1) have an overall preference for the *cis*-(5*R*,6*S*) stereoisomer.[29−31] The endonuclease VIII glycosylase shows a 3.2:1 preference for excising the (5*R*)-Tg vs the (5*S*)-Tg.[29] This is also the case for hNTH1 and hNEIL1 glycosylases: the relative activity for (5*R*)-Tg:(5*S*)-Tg is 13:1 for hNTH1 and 1.5:1 for hNEIL1.[30,31] Similar observations have been made for prokaryotic, tease, and murine glycosylases.[29] In addition, Tg is also repaired by nucleotide excision repair (NER). Both randomly introduced Tg lesions and abasic sites are substrates for the UvrABC repair enzymes of *E. coli*.[32] Subsequently, it was determined that in vitro human NER enzymes excise Tg from DNA through cleaving the N-glycosidic bond.[33]

However, the stability of DNA causes the cleavage of its glycosidic bonds to be a high-energy reaction, which requires catalysis by various enzymes.[31,34,35] Computational chemistry, an important technique to provide more useful information about short-lived transition states that is difficult to obtain from experiments, has been widely used to investigate the N-glycosidic bond cleavage pathways.[36−44] On the basis of the similarities in the proposed mechanisms of the N-glycosidic bond cleavage catalyzed by various enzymes, we desire to study the fundamentals of glycosidic bond cleavage in *cis*-(5*R*,6*S*)-deoxythymidine glycol (*cis*-(5*R*,6*S*)-5,6-dihydroxy-5,6-dihydrodeoxythymidine, dTg) without the action of an enzyme. *cis*-(5*R*,6*S*)-Deoxythymidine glycol was chosen due to its stability,[10−15] its relatively high activity for base excision repair enzymes of Tg,[31−33] and the lack of a systematic study in the literature by proper calculational models for the N-glycosidic bond cleavage process. In the present study, we consider the general mechanisms of unimolecular decomposition as well as the N-glycosidic bond cleavage involving a water nucleophile of dTg. Water was chosen as the nucleophile owing to its important role in the N-glycosidic bond cleavage catalyzed by some enzymes.[28,36,39,41,45−53]

2. Computational Details

As mentioned above, among the four diasteroisomer of dTg, the *cis*-(5*R*,6*S*) conformer is the most stable and is chosen as the reaction system. Geometric structures for all the stationary points, including the reactant complex (RC), product complex (PC), intermediate (IM), and transition state (TS), were optimized in the gas phase using the hybrid density functional theory (BHandHLYP and B3LYP)[54,55] in conjunction with the standard 6-311++G(d,p) basis set containing diffuse functions to provide a sufficient description for the hydrogen-bonded system. The harmonic frequency analysis was used to confirm the stationary point as a minimum with all positive frequencies or as a transition state with only one imaginary frequency. The connectivity between the stationary points was established by intrinsic reaction coordinate (IRC) calculations.[56,57] To obtain more credible energy information, single-point MP2 calculations, MP2/6-311++G(d,p)//BHandHLYP/6-311++G(d,p), were carried out. The natural charges and Wiberg bond orders were calculated for all optimized structures at the BHandHLYP/6-311++G(d,p) level on the basis of the natural bond orbital (NBO) theory.[58,59]

SCHEME 1: Deoxyribose Sugar Models Investigated in the Present Work

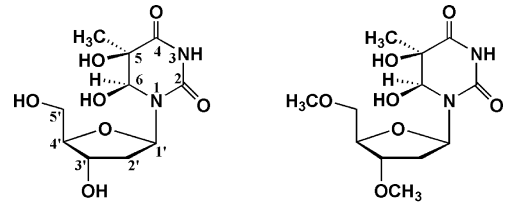

1 **2**

In principle, geometries in solvent should be different from those in the gas phase. We chose water as the solvent to mimic the surroundings of DNA and tried to locate the corresponding stationary points in water with the SCRF method, but failed to get converged results for some structures. Therefore, the solvent effect of water on the four processes was tested by single-point calculation at the geometry optimization level by means of the conductor-like polarized continuum model (CPCM), which has prevailed in the scientific community due to its accuracy and the relative simplicity of the expressions involved in the definition of the solvent reaction field.[60,61] Single-point computation was also done at the MP2/6-311++G(d,p)//BHandHLYP/6-311++G(d,p) level. The dielectric constant used in the calculations is $\varepsilon = 78.4$ for water. Note that all of the single-point energies in water were corrected by the gas-phase thermodynamic quantities. The thermodynamic data reported in this paper are at 298.15 K and 1 atm.

In addition to the level of theory, an appropriate model must be identified to study the N-glycosidic bond cleavage of dTg. To eliminate difficulties associated with modeling charges and conformationally flexible phosphate groups, we focus our attention on two substituted tetrahydrofuran models (see Scheme 1). For deoxythymidine glycol (model **1**), the DNA phosophodiester groups at C3′ and C5′ are replaced with hydroxyl groups. However, Tg exists as stable DNA in the organism. The hydroxyl groups at C3′ and C5′ are inefficient models for DNA phosophodiesters due to their instability caused by the interactions with the nucleobase or nucleophile that do not occur within DNA.[44] Therefore, to investigate the mechanisms of N-glycosidic bond cleavage in the nucleotide, model **2** was established by replacing the hydroxyl groups at C3′ and C5′ with methoxyl groups, which were found to stabilize the relevant structures.[44] We use the smallest nucleoside (model **1**) and nucleotide (model **2**) of dTg for comparison of different reaction pathways of the N-glycosidic bond cleavage. All calculations were carried out by the Gaussian 03 program.[62]

3. Results and Discussion

First, it should be illuminated that all the geometric structures optimized at the BHandHLYP/6-311++G(d,p) and B3LYP/6-311++G(d,p) levels are very similar for the title reaction systems. Compared with the B3LYP/6-311++G(d,p) level, the relative energies calculated at the BHandHLYP/6-311++G(d,p) level are closer to those at the MP2/6-311++G(d,p)//BHandHLYP/6-311++G(d,p) level. Similar results have been reported in the literature[56,63] that the BHandHLYP level has better

SCHEME 2: Four Possible Reaction Pathways for the Glycosidic Bond Cleavage of dTg

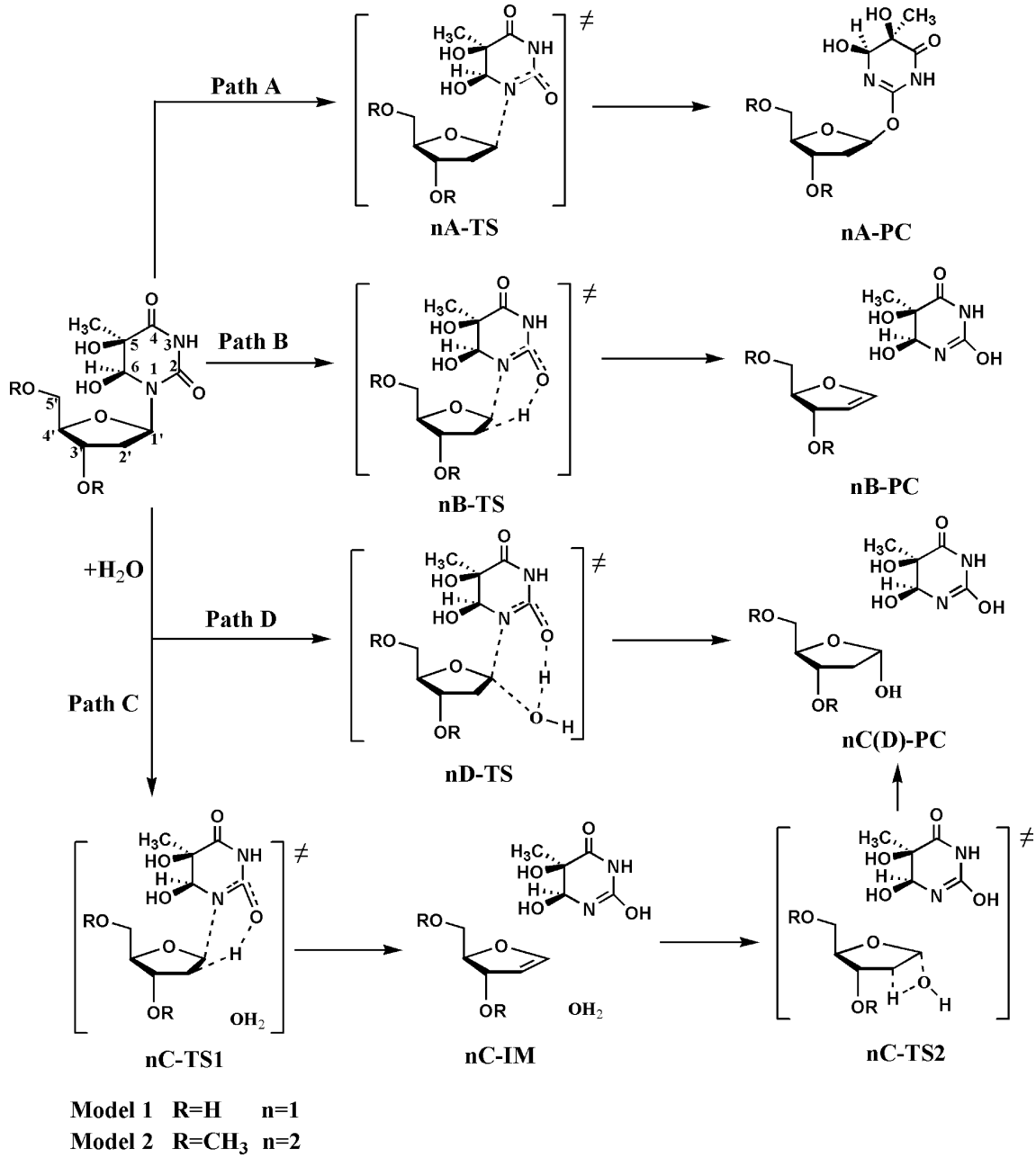

performance in predicting the transition states than other common DFT methods and provides results similar in quality to MP2 results. Recently, two studies have shown that the BHandHLYP level is a viable alternative to the highly correlated quantum chemical methods for calculating the weakly polar interaction energies in polypeptides, and this level has been strongly recommended for the studies of small peptides and other similar biomolecular systems with intramolecular hydrogen bonds.[64,65] Therefore, our discussions here are mainly based on the BHandHLYP/6-311++G(d,p) geometries and energies.

As presented in Scheme 2, we considered four possible reaction pathways, denoted as paths A, B, C, and D. Paths A and B are the unimolecular decomposition reaction mechanisms, corresponding to the direct cleavage and the hydrogen abstraction pathways, respectively. Paths C and D are the two possible hydrolysis mechanisms for the glycosidic bond cleavage. Path C is stepwise, whereas path D is concerted. To facilitate the identification of each transition state and complex in the four pathways, we adopt a nomenclature to characterize each stationary point. As illustrated in Scheme 2, the first number, "*n*", has two values, "1" standing for model **1** and "2" for model **2**. The second letters, "A", "B", "C", and "D", were used to identify the four pathways, i.e., the direct cleavage, the abstraction cleavage, the stepwise S_N1 hydrolysis pathway, and the concerted S_N2 hydrolysis process. For example, the term 1A-TS represents the transition state of model **1** in the direct cleavage pathway (path A), while 2B-TS stands for the transition state of model **2** of the abstraction cleavage pathway (path B). The atomic numbering of the system involved in the center of the reactions is given in the figures displaying the corresponding optimized structures.

3.1. Comparison of the Theoretical Geometry and Crystal Structure of dTg. The optimized geometry of deoxythymidine glycol at the BHandHLYP/6-311++G(d,p) level is presented in Figure 1. As depicted in Figure 1, the deoxythymidine glycol has C3′-*endo* sugar puckering, which is the naturally occurring

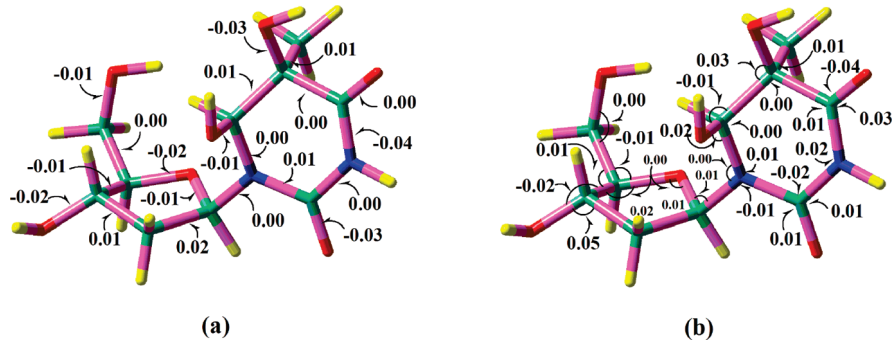

Figure 1. Relative deviations of bond lengths (a) and bond angles (b) between the crystal structure and theoretical geometry optimized at the BHandHLYP/6-311++G(d,p) level for deoxythymidine glycol.

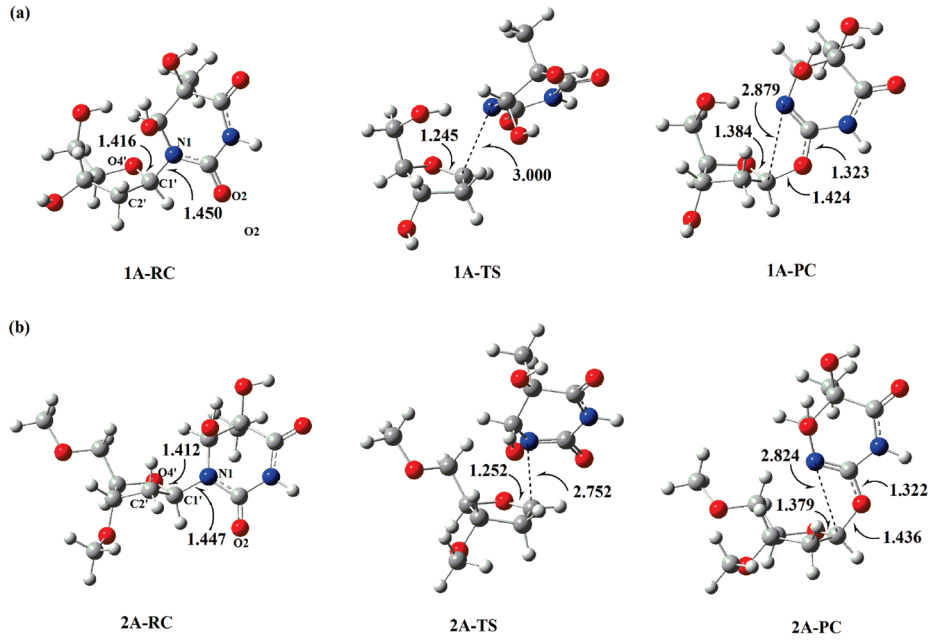

Figure 2. Optimized structures of the stationary points for models **1** (a) and **2** (b) in the direct cleavage pathway (path A) at the BHandHLYP/6-311++G(d,p) level (bond length in angstroms).

conformation in DNA.[66] The pyrimidine ring of Tg exhibits an approximate half-chair conformation. The best contiguous four-atom plane is defined by the N1, C2, N3, and C4 atoms. In this conformation, the 5-methyl and 6-hydroxyl groups occupy pseudoaxial positions whereas the 5-hydroxyl group is preudoequatorial and *gauche* to the 6-hydroxyl. The torsion angles χ ($\angle$(O4′−C1′−N1−C2) = −128.2°) and χ' ($\angle$(O4′−C1′−N1−C6) = 63.7°) show that thymine glycol has the *anti* conformation about the N-glycosyl bond. These structural features agree well with the X-ray crystallographic structure[67,68] and the ab initio calculation geometries.[69] In addition, the differences in the bond lengths, bond angles, and torsion angles between the crystal structure and theoretical geometry optimized at the BHandHLYP/6-311++G(d,p) level are given in Figure 1 and Tables S1−S3 in the Supporting Information. These differences are very small with a relative deviation of less than 5% except for the torsion angle χ (with a relative deviation of 14%), attributed to the presence of intermolecular interactions in the crystal. Therefore, it seems that the BHandHLYP/6-311++G(d,p) approach is acceptable for this work.

3.2. Unimolecular N-Glycosidic Bond Cleavage. It has been well-documented that the hydrolysis or enzymatic catalysis is essential to the N-glycosidic bond cleavage in nucleotides because of their high stability.[31,34] However, it is still of interest to investigate the unimolecular decomposition of dTg in the absence of any external force to gain a greater understanding of the glycosidic bond cleavage process. Two decomposition pathways were characterized in the gas phase, denoted as the direct cleavage pathway (path A) and abstraction cleavage pathway (path B).

3.2.1. Direct Cleavage Pathway (Path A). In the gas phase, the potential energy surface for the direct cleavage of the C1′−N1 N-glycosidic bond reveals a possible transition state. The optimized geometries and important bond lengths for the stationary points are shown in Figure 2. The vector of the imaginary vibrational frequency in the transition state mainly corresponds to the cleavage of the C1′−N1 bond. The distances of the C1′−N1 bond in 1A-TS and 2A-TS are 3.000 and 2.752 Å, respectively, longer than those in the reactants (1.450 Å for 1A-RC and 1.447 Å for 2A-RC), suggesting that the N-glycosidic bond has almost broken in the transition state. The hybridization of C1′ converts from sp^3 in the reactant to sp^2, and the C1′−O4′ single bond turns to a double bond (1.416 Å in 1A-RC vs 1.245 Å in 1A-TS and 1.412 Å in 2A-RC vs 1.252 Å in 2A-TS). Owing to the instability of the (charge) separated sugar cation and base anion in the gas phase, the nucleobase rotates to coordinate O2 to the C1′ atom following the cleavage of the glycosidic bond, leading to the formation of the C1′−O2 bond in the product. In 1A-PC and 2A-PC, the C1′−O4′ single bond is restored (1.384 Å in 1A-PC and 1.379 Å in 2A-PC);

TABLE 1: Changes of the Free Energies and Electronic Energies for the Four Pathways in the Gas Phase and Water (kcal/mol)

	BHandHLYP/6-311++G(d,p)				MP2/6-311++G(d,p)// BHandHLYP/6-311++G(d,p)			
	ΔG(gas)	ΔG(sol)	ΔE(gas)	ΔE(sol)	ΔG(gas)	ΔG(sol)	ΔE(gas)	ΔE(sol)
Direct Cleavage Pathway								
1A-RC → 1A-TS	47.42	41.56	46.68	40.82	50.91	44.65	50.17	43.91
1A-RC → 1A-PC	20.80	20.58	19.58	19.36	23.01	22.35	21.79	21.13
2A-RC → 2A-TS	51.66	49.29	52.00	49.62	56.34	50.58	53.88	50.92
2A-RC → 2A-PC	23.46	24.65	23.28	24.47	25.15	25.62	24.78	25.44
Abstraction Cleavage Pathway								
1B-RC → 1B-TS	46.01	45.54	47.24	46.77	46.50	45.75	47.73	46.98
1B-RC → 1B-PC	22.38	20.16	26.76	24.53	25.74	23.09	30.12	27.47
2B-RC → 2B-TS	44.56	39.97	45.14	40.55	45.51	40.89	46.10	41.48
2B-RC → 2B-PC	16.74	15.11	19.10	17.47	20.23	18.31	22.59	20.68
S_N1 Hydrolysis Pathway								
1C-RC → 1C-TS1	45.62	45.23	46.42	46.03	45.72	44.98	46.52	45.78
1C-RC → 1C-IM	20.65	19.66	25.23	24.24	23.72	22.35	28.30	26.93
1C-IM → 1C-TS2	55.12	46.06	51.73	42.67	54.12	45.25	50.73	41.86
1C-IM → 1C-PC	−14.04	−10.12	−18.48	−14.57	−13.27	−9.62	−17.71	−14.07
1C-RC → 1C-PC	6.61	9.54	6.75	9.67	10.45	12.73	10.59	12.86
2C-RC → 2C-TS1	44.06	41.26	44.38	41.58	44.09	40.93	44.41	41.25
2C-RC → 2C-IM	16.41	15.98	18.50	18.07	20.68	19.70	22.77	21.79
2C-IM → 2C-TS2	54.36	49.58	52.42	47.63	53.66	49.21	51.71	47.26
2C-IM → 2C-PC	−10.28	−9.84	−12.50	−12.06	−10.37	−9.99	−12.60	−12.22
2C-RC → 2C-PC	6.13	6.14	6.00	6.01	10.31	9.71	10.17	9.57
S_N2 Hydrolysis Pathway								
1D-RC → 1D-TS	47.52	43.66	47.39	43.53	50.56	46.20	50.42	46.07
1D-RC → 1D-PC	12.19	10.02	14.28	12.10	17.61	15.23	19.70	17.31
2D-RC → 2D-TS	48.03	41.37	48.78	42.10	53.04	45.98	53.80	46.74
2D-RC → 2D-PC	15.61	13.44	16.21	14.02	20.64	18.29	21.24	18.89

the lengths of the C1′−O2 bonds are 1.424 and 1.436 Å, respectively.

Despite the promise of this transition structure in the direct cleavage, this is a high-energy process. The changes in the free energies (ΔG) and electronic energies (ΔE) are given in Table 1. As shown in Table 1, the free energy barriers of 1A-TS and 2A-TS at the BHandHLYP/6-311++G(d,p) level are 47.42 and 51.66 kcal/mol, respectively, which increase to 50.91 and 56.34 kcal/mol at the MP2/6-311++G(d,p)//BHandHLYP/6-311++G(d,p) level, respectively. Moreover, the reaction is largely endothermic (with reaction energies of 20−26 kcal/mol).

3.2.2. Abstraction Cleavage Pathway (Path B). Further searches of the potential energy surface for the unimolecular decomposition reaction reveal the second possible transition state. All the optimized structures of the reactants, transition states, and products are presented in Figure 3. The vector of the imaginary vibrational frequency for the transition state mainly corresponds to the proton (H2′) transfer from the C2′ atom to the O2 atom, which is favorable in the gas phase to stabilize a partial negative charge on the base and a partial positive charge on the sugar. The distances of C1′−N1, O2−H2′, and C2′−H2′ in 1B-TS of model **1** are 2.699, 1.345,

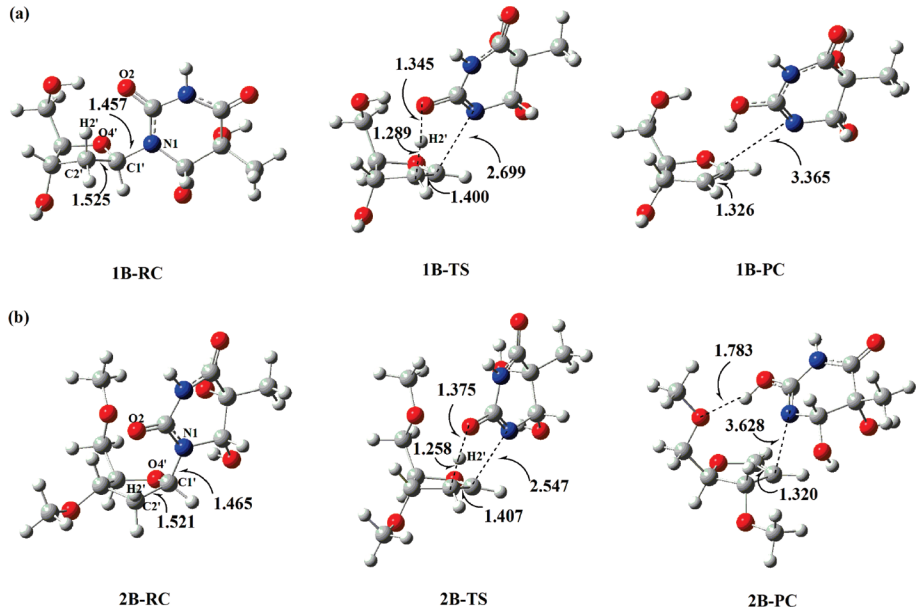

Figure 3. Optimized structures of the stationary points for models **1** (a) and **2** (b) in the abstraction cleavage pathway (path B) at the BHandHLYP/6-311++G(d,p) level (bond length in angstroms).

and 1.289 Å, respectively. For model **2**, the corresponding lengths of the three bonds in 2B-TS are 2.547, 1.375, and 1.258 Å, respectively. The distances of C1′−C2′ in 1B-TS and 2B-TS are 1.400 and 1.407 Å, respectively, shorter than those in the reactants (1.525 Å in 1B-RC and 1.521 Å in 2B-RC). This indicates that the C1′−C2′ bond become stronger because of the partial cleavages of the C1′−N1 and C2′−H2′ bonds. In the product, the H2′ atom is completely abstracted by the nucleobase. The hybridizations of the C1′ and C2′ atoms convert from sp^3 in the reactants to sp^2, leading to the formation of a C1′═C2′ bond (1.326 Å in 1B-PC and 1.320 Å in 2B-PC), which flattens the sugar ring. In 1B-PC and 2B-PC, the nucleobase remains coordinated to the sugar moiety through a weak interaction with the newly formed C1′−C2′ double bond in 1B-PC and a stronger (O5′···H−O2) hydrogen bond in 2B-PC.

Although the computational literature[37] has reported the transition state involving C2′−H abstraction, there is little experimental evidence for the existence of the high-energy glycal intermediate formed in the glycosidic bond cleavages process within nucleotides. To our best knowledge, only one report was found to concern a ribal moiety as a minor product in an enzymatic reaction.[65] Our computational results show that the abstraction cleavage process is still a high-energy process. The relative free energies and electronic energies are presented in Table 1. As described in Table 1, the free energy barriers of 1B-TS and 2B-TS calculated at the BHandHLYP/6-311++G(d,p) level are 46.01 and 44.56 kcal/mol, respectively, slightly lower than those at the MP2/6-311++G(d,p)//BHandHLYP/6-311++G(d,p) level (46.50 kcal/mol for 1B-TS and 45.51 kcal/mol for 2B-TS). Likewise, the whole reaction is still largely endothermic with reaction energies of 16−26 kcal/mol.

In summary, it is clear from our computation that the cleavage of the N-glycosidic bond via unimolecular decomposition is not feasible, which is in agreement with experimental results that the nonenzymatic glycosidic bond cleavage occurs via hydrolysis and emphasizes the significant role of the nucleophile. We therefore turn our attention to the hydrolysis of the glycosidic bond of dTg.

3.3. Direct Hydrolysis of the Glycosidic Bond. A variety of nucleophiles (water, amines, and phosphates) have been involved in the N-glycosidic bond cleavage of nucleotides. However, water is present in the active sites of many enzymes that catalyze the N-glycosidic bond cleavage reactions.[36,38,41,45−53] Therefore, we investigated the role of water in the N-glycosidic bond cleavage of dTg. On the basis of the proposed mechanisms for many of the enzymatic glycosidic bond cleavages, two possible reaction mechanisms, S_N1 (path C) and S_N2 (path D), were considered to investigate the role of nucleophile water in the glycosidic bond cleavage of dTg.

3.3.1. S_N1 Pathway (Path C). This possible pathway is actually a two-step process: the H2′ atom at first is abstracted by the O2 atom of the nucleobase with the simultaneous cleavage of the glycosidic bond to form a glycal intermediate; then the water adds across the C1′═C2′ bond, which restores the C2′ hydrogen. All of the relevant structures are presented in Figure 4. We note, however, that there is no experimental evidence for abstraction of a (C2′) sugar hydrogen during the hydrolysis of deoxynucleosides, which indicates that another pathway predominates.

In the first step, the vector of the imaginary vibrational frequency for the transition state mainly corresponds to the proton (H2′) transfer from the C2′ atom to the O2 atom. The distances of C1′−N1, O2−H2′, and C2′−H2′ in 1C-TS1 are 2.762, 1.325, and 1.303 Å, respectively. For 2C-TS1, the lengths of the three bonds correspond to 2.609, 1.368, and 1.263 Å, respectively. The distances of C1′−C2′ in 1C-TS1 and 2C-TS1 are 1.399 and 1.406 Å, respectively, shorter than those in the reactants (1.527 Å for 1C-RC and 1.518 Å for 2C-RC). In 1C-IM and 2C-IM, the proton H2′ is completely transferred from the C2′ atom to the O2 atom. The distances of C1′−N1 are 3.337 and 3.187 Å, respectively, implying that the C1′−N1 bond has already been broken. The hybridizations of the C1′ and C2′ atoms convert from sp^3 in the reactant to sp^2; the C1′−C2′ bond changes from a single bond in the reactants to a double bond (1.328 Å in 1C-IM and 1.323 Å in 2C-IM).

In the second step, the water adds across the C1′═C2′ bond to form the product via the four-membered transition state. The distances of C1′−O, O−H1, H1−C2′, and C1′−C2′ in 1C-TS2 are 2.774, 1.743, 1.129, and 1.431 Å, respectively. For 2C-TS2, the corresponding lengths of the four bonds are 2.237, 1.389, 1.238, and 1.421 Å, respectively. The analysis of the vibrational frequency of the transition state indicates that it mainly corresponds to the proton (H1) transfer from water to the C2′ atom. After the transition states 1C-TS2 and 2C-TS2 are overcome, the products 1C-PC and 2C-PC are produced. In 1C-PC and 2C-PC, the nucleobase remains bonded with the sugar through strong hydrogen bonds, O···H−O4 and O4′···H−N3 in 1C-PC and O5′···H−O2 in 2C-PC. The lengths of the C1′−C2′ bonds are 1.511 and 1.526 Å, respectively, which shows that the C1′−C2′ bond becomes weaker and changes from a double bond to a single bond.

The relative free energies and electronic energies are shown in Table 1. There are two high peaks on the potential energy surface. For model **1**, the free energy barriers of 1C-TS1 and 1C-TS2 are 45.62 and 55.12 kcal/mol, respectively, at the BHandHLYP/6-311++G(d,p) level, which are higher than those in model **2** (44.06 kcal/mol for 2C-TS1 and 54.36 kcal/mol for 2C-TS2). For the MP2 single-point calculation, the free energy barriers of 1C-TS1, 1C-TS2, 2C-TS1, and 2C-TS2 are 45.72, 54.12, 44.09, and 53.66 kcal/mol, respectively. The high free energy barriers indicate that the S_N1 pathway is not favorable to the cleavage of the N-glycosidic bond in dTg.

3.3.2. S_N2 Pathway (Path D). The alternative hydrolysis pathway characterized in the present work is a one-step (S_N2) reaction. As the reaction proceeds, Tg abstracts a proton from water, while the remaining hydroxyl anion adds to the C1′ atom. The corresponding geometries are presented in Figure 5. In this pathway, the vector of the imaginary vibrational frequency of the transition state is mainly associated with the motions of a proton (H1) from water to the O2 atom and the O atom from water to the C1′ atom. The distances of C1′−O, O−H1, H1−O2, and C1′−N1 in 1D-TS are 2.512, 0.978, 1.759, and 2.752 Å, respectively, which correspond to 2.522, 0.975, 1.715, and 2.809 Å, respectively, in 2D-TS. In the product, the nucleobase interacts with the sugar through strong hydrogen bonds, including O2−H···O and O−H···N1 in 1D-PC and O2−H···O in 2D-PC.

The relative free energies of all optimized structure are given in Table 1. The S_N2 pathway is also associated with a large reaction barrier. The free energy barriers of 1D-TS1 and 2D-TS1 are 47.52 and 48.03 kcal/mol, respectively, at the BHandHLYP/6-311++G(d,p) level. At the MP2 single-point calculation, the free energy barriers increase to 50.56 and 53.04 kcal/mol, respectively.

The calculated total relative energy profiles of unimolecular decomposition and hydrolysis of dTg are presented in Figures

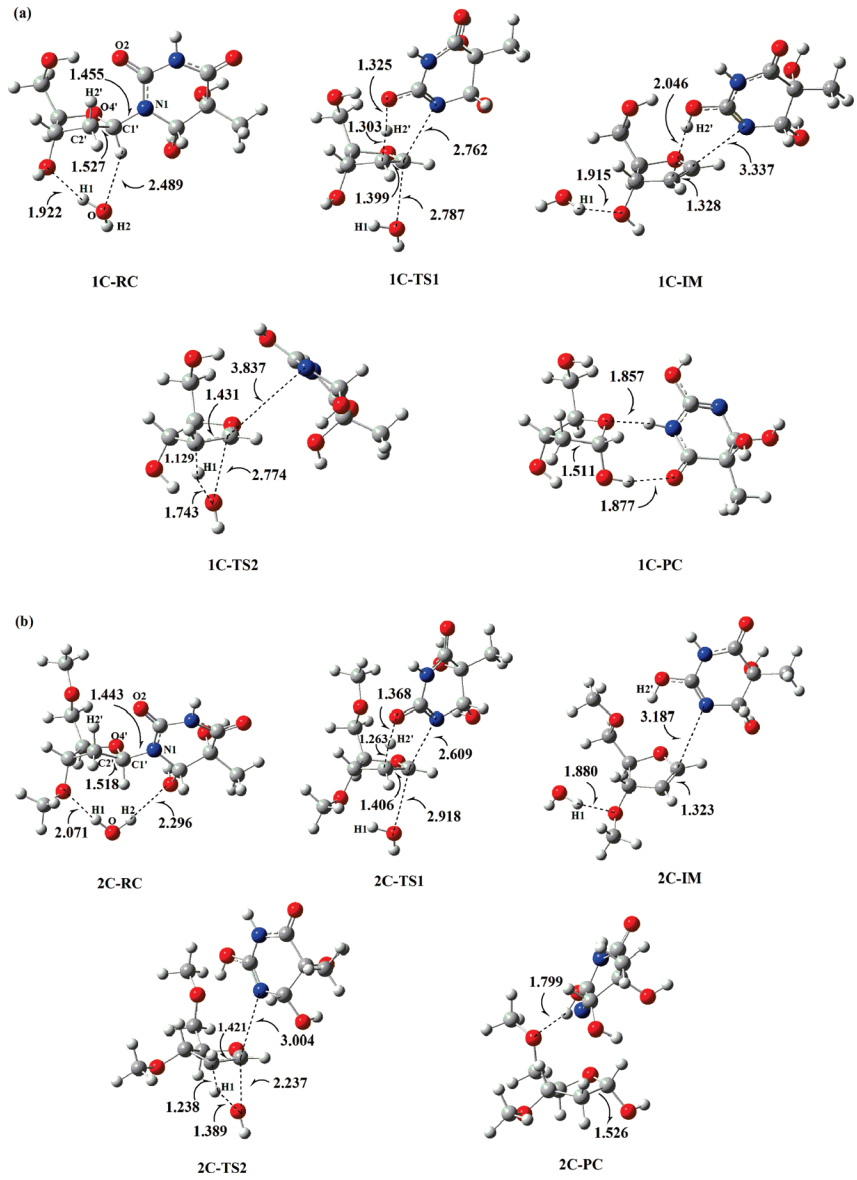

Figure 4. Optimized structures of the stationary points for models **1** (a) and **2** (b) in the S_N1 pathway (path C) at the BHandHLYP/6-311++G(d,p) level (bond length in angstroms).

6 (model **1**) and 7 (model **2**). As depicted in Figures 6 and 7, although nucleophile water has been implicated in the glycosidic bond cleavage of nucleotides, the reaction barriers for both hydrolysis pathways do not differ significantly from those for the unimolecular decomposition reaction in the gas phase. The large barriers calculated indicate that the role of water as outlined in the above mechanisms is not beneficial to the N-glycosidic bond cleavage of dTg and therefore the direct involvement of a single water molecule as a nucleophile is improbable. This result emphasizes the important role of enzymes.

3.4. Solvent Effect. In fact, the N-glycosidic bond cleavage is the first crucial step occurring in DNA to remove the oxidative base, so it is of interest to study the influence of the solvent effect on the energies and mechanisms of the glycosidic bond cleavage of dTg. Water was chosen as a neutral solvent in our calculation. We performed the single-point energy computations at the CPCM-BHandHLYP/6-311++G(d,p) and CPCM-MP2/6-311++G(d,p) levels on the basis of the gas-phase geometries optimized at the BHandHLYP/6-311++G(d,p) level. Computed single-point energies for all the critical structures in a medium of water are presented in Table 1 and are compared with the corresponding gas-phase values.

For the direct cleavage pathway, in model **1**, the dipole moment of 1A-TS (8.1216 D) is larger than that of 1A-RC (1.4473 D), and then the solvation of water on 1A-TS is stronger than that on 1A-RC. As a result, the solvent water stabilizes the transition state 1A-TS, leading to a reduction of the energy barrier. The free energy barrier of 1A-TS in water is decreased by 5.86 kcal/mol at the BHandHLYP/6-311++G(d,p) level and by 6.26 kcal/mol at the MP2/6-311++G(d,p) level. For model **2**, the free energy barriers in water are 2.37 and 5.76 kcal/mol lower than those in the gas phase at the BHandHLYP/6-311++G(d,p) and MP2/6-311++G(d,p) levels, respectively, ascribed to the larger dipole moment of 2A-TS (6.5556 D) as compared with that of 2A-RC (3.8425 D).

Considering the abstraction cleavage pathway, the stabilization of the transition state by the solvent water is favorable to a decrease of the energy barrier in water. However, the dipole moment of 1B-TS (4.3422 D) is only 0.2775 D larger than that of 1B-RC (4.0647 D), which just causes a slight reduction of the free energy barrier in water by 0.47 kcal/mol at the BHandHLYP/6-311++G(d,p) level and 0.75 kcal/mol at the MP2/6-311++G(d,p) level. In contrast, for model **2**, the large dipole moment difference (4.6236 D) between 2B-TS (5.6405

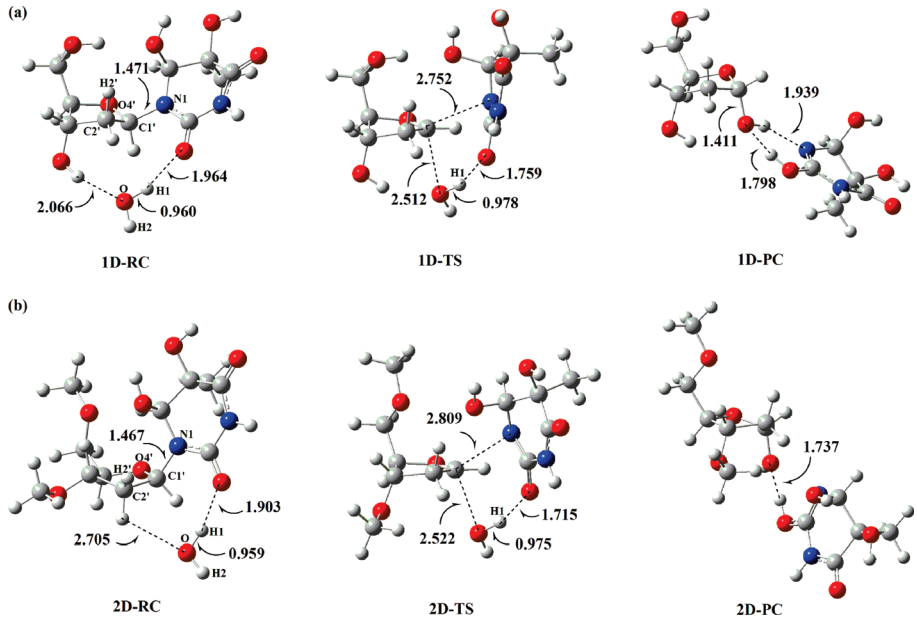

Figure 5. Optimized structures of the stationary points for models **1** (a) and **2** (b) in the S_N2 pathway (path D) at the BHandHLYP/6-311++G(d,p) level (bond length in angstroms).

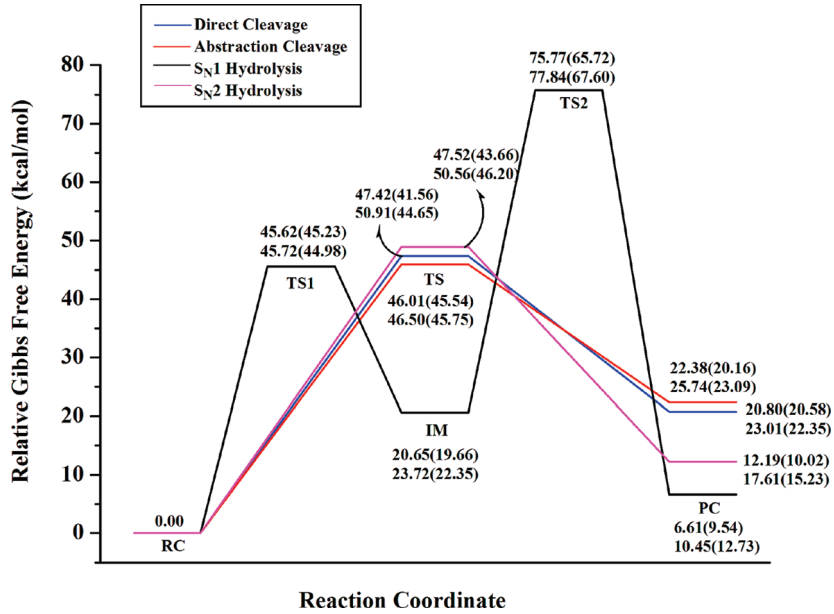

Figure 6. Potential energy profile along the four pathways of model **1** (top values, ΔG at the BHandHLYP/6-311++G(d,p) level in the gas phase; bottom values, ΔG at the MP2/6-311++G(d,p)//BHandHLYP/6-311++G(d,p) level in gas; values in parentheses, ΔG in water at the corresponding calculation level).

D) and 2B-RC (1.0169 D) accounts for the remarkable reduction of the free energy barrier in water by 4.59 and 4.62 kcal/mol at the BHandHLYP/6-311++G(d,p) and MP2/6-311++ G(d,p) levels, respectively.

For the S_N1 pathway, the first energy barriers of model **1** in water are 0.39 and 0.74 kcal/mol lower than those in the gas phase at the BHandHLYP/6-311++G(d,p) and MP2/6-311++G(d,p) levels, respectively, attributed to the fact that the dipole moment of 1C-TS1 (6.1289 D) is larger than that of 1C-RC (2.9592 D). For model **2**, the larger dipole moment of 2C-TS1 (7.7702 D) compared to that of 2C-RC (2.2293 D) accounts for the reduction of the free energy barrier in water (with decreased values of 2.80 and 3.16 kcal/mol at the BHandHLYP/6-311++G(d,p) and MP2/6-311++G(d,p) levels, respectively). In the second step, the dipole moment of 1C-TS2 is 6.9681 D, 5.6159 D larger than that of 1C-IM (1.3522 D), whereas for model **2**, the dipole moment difference between 2C-TS2 (5.5651 D) and 2C-IM (2.6009 D) is 2.9642 D, smaller than that of model **1**, which leads to a lower reduction of the free energy barrier in model **2**. Computational results show that the free energy barriers of 1C-TS2 in water are decreased by 9.06 and 8.87 kcal/mol at the BHandHLYP/6-311++G(d,p) and MP2/6-311++G(d,p) levels, respectively, larger than those of 2C-TS2 (4.78 kcal for the BHandHLYP/6-311++G(d,p) level and 4.45 kcal/mol for the MP2/6-311++G(d,p) level).

Finally, the S_N2 pathway is considered. The dipole moments of 1D-TS (5.7763 D) and 2D-TS (10.0671 D) are both larger than those of their own reactants (3.7478 D for 1D-RC and 2.7456 D for 2D-RC). For model **1**, the free energy barrier in water is 3.86 kcal/mol lower than that in the gas phase at the BHandHLYP/6-311++G(d,p) level, which corresponds to 4.36 kcal/mol at the MP2/6-311++G(d,p) level. For model **2**, the

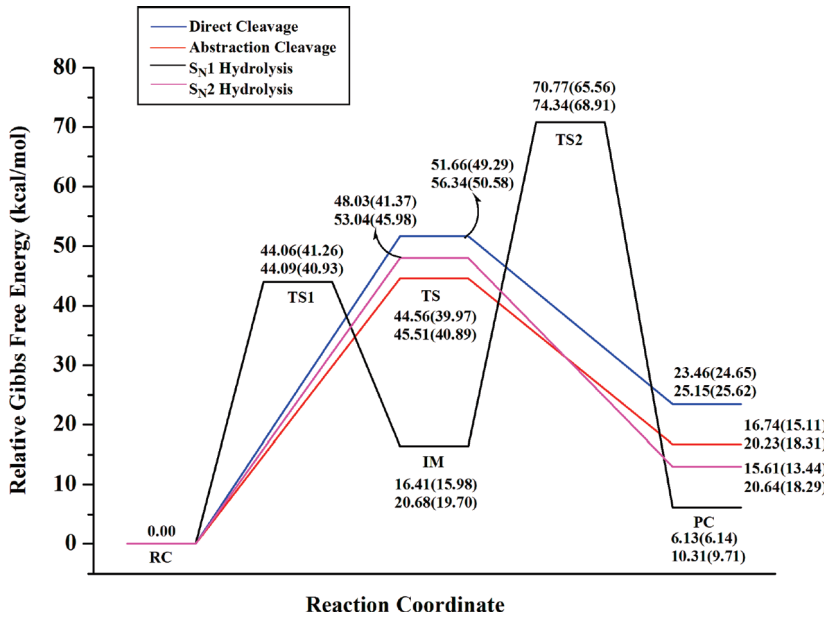

Figure 7. Potential energy profile along the four pathways of model **2** (top values, ΔG at the BHandHLYP/6-311++G(d,p) level in the gas phase; bottom values, ΔG at the MP2/6-311++G(d,p)//BHandHLYP/6-311++G(d,p) level in gas; values in parentheses, ΔG in water at the corresponding calculation level).

TABLE 2: Natural Charges (q) and Changes in Charges (Δq) in the Four Pathways at the BHandHLYP/6-311++G(d,p) Level (electronic charge units)

direct cleavage pathway				S_N1 hydrolysis pathway							
	C1′	N1	O2		C1′	C2′	N1	O2	H2′	O	H1
$q^{1A\text{-}RC}$	0.355	−0.576	−0.652	$q^{1C\text{-}RC}$	0.337	−0.433	−0.574	−0.701	0.234	−0.954	0.484
$\Delta q^{1A\text{-}TS}$	0.251	−0.265	−0.130	$\Delta q^{1C\text{-}TS1}$	0.221	−0.178	−0.140	−0.115	0.187	0.003	0.003
$\Delta q^{1A\text{-}PC}$	0.138	−0.097	0.067	$\Delta q^{1C\text{-}IM}$	−0.114	0.026	−0.064	0.001	0.280	−0.004	0.003
$q^{2A\text{-}RC}$	0.353	−0.573	−0.652	$q^{1C\text{-}IM}$	0.223	−0.407	−0.638	−0.701	0.514	−0.958	0.487
$\Delta q^{2A\text{-}TS}$	0.262	−0.239	−0.134	$\Delta q^{1C\text{-}TS2}$	0.382	−0.180	0.020	−0.017	−0.007	−0.318	−0.100
$\Delta q^{2A\text{-}PC}$	0.140	−0.074	0.059	$\Delta q^{1C\text{-}PC}$	0.236	−0.025	0.018	0.008	−0.016	0.162	−0.264
				$q^{2C\text{-}RC}$	0.344	−0.427	−0.577	−0.657	0.262	−0.951	0.475
				$\Delta q^{2C\text{-}TS1}$	0.236	−0.196	−0.170	−0.109	0.158	0.000	0.007
				$\Delta q^{2C\text{-}IM}$	−0.098	0.049	−0.055	−0.065	0.266	−0.008	0.009
				$q^{2C\text{-}IM}$	0.246	−0.378	−0.632	−0.722	0.528	−0.959	0.484
				$\Delta q^{2C\text{-}TS2}$	0.337	−0.237	−0.014	0.002	−0.002	−0.199	−0.060
				$\Delta q^{2C\text{-}PC}$	0.214	−0.062	−0.014	0.002	0.005	0.207	−0.268

abstraction cleavage pathway						S_N2 hydrolysis pathway					
	C1′	N1	C2′	O2	H2′		C1′	N1	O2	O	H1
$q^{1B\text{-}RC}$	0.347	−0.577	−0.429	−0.697	0.234	$q^{1D\text{-}RC}$	0.361	−0.566	−0.709	−0.973	0.502
$\Delta q^{1B\text{-}TS}$	0.191	−0.145	−0.178	−0.115	0.183	$\Delta q^{1D\text{-}TS}$	0.231	−0.218	−0.111	−0.017	0.024
$\Delta q^{1B\text{-}PC}$	−0.131	−0.059	0.041	−0.008	0.280	$\Delta q^{1D\text{-}PC}$	0.098	−0.119	0.003	0.129	0.025
$q^{2B\text{-}RC}$	0.353	−0.588	−0.425	−0.675	0.236	$q^{2D\text{-}RC}$	0.359	−0.567	−0.708	−0.958	0.492
$\Delta q^{2B\text{-}TS}$	0.200	−0.159	−0.192	−0.087	0.183	$\Delta q^{2D\text{-}TS}$	0.274	−0.215	−0.125	−0.018	0.025
$\Delta q^{2B\text{-}PC}$	−0.142	−0.053	0.084	−0.043	0.293	$\Delta q^{2D\text{-}PC}$	0.114	−0.085	−0.006	0.164	0.046

decreased values of the free energy barriers in water are 6.66 and 7.06 kcal/mol at the BHandHLYP/6-311++G(d,p) and MP2/6-311++G(d,p) levels, respectively, which are more than those in model **1** due to its larger dipole moment difference between the transition state and the reactant.

Additionally, it is well-known that chemical reactions are closely involved in the charge distributions. The preference of unimolecular decomposition and direct hydrolysis of dTg was further analyzed by the NPA charge distribution from the NBO method at the BHandHLYP/6-311++G(d,p) level. The atomic charge distributions of the unimolecular decomposition reaction and hydrolysis are presented in Table 2. The chosen atoms in the tables are directly involved in the reactions or are expected to be involved. From the charge distribution, we can qualitatively explain the decrease of the free energies in water. As shown in Table 2, for the four processes, the charge distributions at the transition states are centralized, which is favorable to an increase of the stability of the transition states in water due to the strong electrostatic interactions with the solvent water. The high stability of the transition states in water inevitably leads to a reduction of the free energy barriers.

As a result, the solvation of water contributes to lowering all the free energy barriers in the four pathways. It is shown that the direct cleavage pathway is favored for the N-glycosidic bond cleavage of model **1** due to the minimum free energy barrier of 44.65 kcal/mol in water at the MP2 single calculation level. For model **2**, however, the most favorable pathway is the abstraction cleavage process with a minimum free energy barrier of 40.89 kcal/mol in water at the MP2/6-311++G(d,p) level. Therefore, the presence of the nucleophile water is not beneficial

TABLE 3: Percentage of Evolution of Bond Orders (E_v, %) and Synchronicity (S_y) in the Four Pathways

	bond	E_v (%)	S_y
Direct Cleavage Pathway			
1A-RC → 1A-TS → 1A-PC	C1′−N1	99.11	0.09
	C1′−O2	4.48	
2A-RC → 2A-TS → 2A-PC	C1′−N1	95.49	0.16
	C1′−O2	8.03	
S_N1 Hydrolysis Pathway			
1C-RC → 1C-TS1 → 1C-IM	C1′−N1	95.83	0.72
	C2′−H2′	48.84	
	O2−H2′	38.48	
1C-IM → 1C-TS2 → 1C-PC	C1′−O	5.94	0.55
	C2′−H1	76.99	
	O−H1	90.35	
2C-RC → 2C-TS1 → 2C-IM	C1′−N1	92.59	0.69
	C2′−H2′	43.28	
	O2−H2′	36.61	
2C-IM → 2C-TS2 → 2C-PC	C1′−O	23.29	0.73
	C2′−H1	57.64	
	O−H1	69.57	
Abstraction Cleavage Pathway			
1B-RC → 1B-TS → 1B-PC	C1′−N1	94.75	0.71
	C2′−H2′	47.37	
	O2−H2′	37.09	
2B-RC → 2B-TS → 2B-PC	C1′−N1	89.98	0.71
	C2′−H2′	44.05	
	O2−H2′	36.37	
S_N2 Hydrolysis Pathway			
1D-RC → 1D-TS → 1D-PC	C1′−N1	94.60	0.34
	O−H1	8.13	
	C1′−O	6.59	
	O2−H1	5.31	
2D-RC → 2D-TS → 2D-PC	C1′−N1	98.32	0.40
	O−H1	17.97	
	C1′−O	5.37	
	O2−H1	7.07	

to the cleavage of the glycosidic bond in dTg, which suggests that the enzymatic catalysis is essential to the glycosidic bond cleavage.

3.5. Bond Order Analysis. To gain insight into the various bond-breaking or bond-making processes, the Wiberg bond order values were obtained through NBO analysis at the BHandHLYP/6-311++G(d,p) level in the gas phase. The percentage of evolution of bond orders (E_v, %) is given by

$$E_v\,(\%) = \frac{B_i^{TS} - B_i^{RC}}{B_i^{PC} - B_i^{RC}} \times 100 \qquad (1)$$

In the equation, B is the bond order and the superscripts TS, RC, and PC denote the transition state, reactant complex, and product complex, respectively. The average percentage of evolution of bond orders [$(E_v)_{av}$, %] is offered by

$$(E_v)_{av}\,(\%) = n^{-1}\sum_{i=1}^{n}[(E_v)_i\,(\%)] \qquad (2)$$

where n refers to the number of bonds directly involved in the reaction.

Another concept, synchronicity (S_y), proposed by Moyano et al.,[71] is used to describe the global nature of bond-breaking/forming processes in the decomposition reaction and is expressed by

$$S_y = 1 - \frac{\sum_{i=1}^{n}\frac{|[(E_v)_i\,(\%)] - [(E_v)_{av}\,(\%)]|}{(E_v)_{av}\,(\%)}}{2n-2} \qquad (3)$$

The related percentage of evolution of bond orders (E_v) and synchronicity (S_y) in the four pathways for models **1** and **2** are presented in Table 3. As illustrated in Table 3, the results of model **1** from bond order calculation are similar to those of model **2**. Therefore, we focus our following discussion on the results of model **1**.

For model **1**, in the direct cleavage reaction, the C1′−N1 bond cleavage (E_v = 99.11%) is more advanced than the C1′−O2 bond formation (E_v = 4.48%), which is favorable to stabilizing the separated sugar cation and base anion. It is just the C1′−N1 bond cleavage that leads to the C1′−O2 bond formation. Therefore, this process is completely asynchronous, the synchronicity value being 0.09 for model **1**. For the abstraction cleavage pathway, the most advanced step is still the C1′−N1 bond cleavage (E_v = 94.75%). The C2′−H2′ bond cleavage (E_v = 47.37%) and O2−H2′ bond formation (E_v = 37.09%) are almost a simultaneous process, which corresponds to the transfer of the H2′ atom from C2′ to O2. The synchronicity value of 0.71 for model **1** reveals that the abstraction mechanism is slightly asynchronous.

Considering the S_N1 hydrolysis pathway, the bond-breaking and bond-making orders in step 1 are similar to those of the abstraction cleavage pathway. The C1′−N1 bond cleavage (E_v = 95.83%) is the most advanced among all bond-breaking/making processes. The C2′−H2′ bond cleavage (E_v = 48.84%) and O2−H2′ bond formation (E_v = 38.48%) are almost a simultaneous process. The synchronicity value of model **1** is 0.72, suggesting that this process is slightly asynchronous. In step 2, the cleavage of the O−H1 bond (E_v = 90.35%) is very early. The C2′−H1 bond formation (E_v = 76.99%) is more advanced than the C1′−O bond formation (E_v = 5.94%), which corresponds to the addition of water to the C1′=C2′ bond. This indicates that the H1 transfer is earlier than the O transfer. The synchronicity value of 0.55 for model **1** shows that the second step is still an asynchronous process. As far as the S_N2 process is concerned, the C1′−N1 bond cleavage (E_v = 94.60%) is the most advanced among all of the processes. The O−H1 bond cleavage (E_v = 8.13%), C1′−O bond formation (E_v = 6.59%), and O2−H1 bond formation (E_v = 5.31%) are almost a simultaneous process, which corresponds to the nucleophilic attack of water on the C1′ atom with the simultaneous proton transfer from water to the O2 atom. The small synchronicity value, 0.34, for model **1** indicates that the S_N2 process is still asynchronous.

The results of bond order calculation confirm that models **1** and **2** have the same order of bond cleavage/formation in the four pathways and that all the processes are asynchronous.

4. Conclusions

The cleavage of the N-glycosidic bonds is an important biological process, including DNA repair and nucleotide salvage pathways. In the present work we studied the kinetics and thermodynamics of the N-glycosidic bond cleavage in the smallest nucleoside (model **1**) and nucleotide (model **2**) of dTg by means of computational chemistry. The most favorable route for the unimolecular glycosidic bond cleavage in dTg in the gas phase was characterized to involve the abstraction of a (C2′) sugar hydrogen by the nucleobase. However, this reaction pathway is associated with a large barrier and endothermic reaction energy. Furthermore, no experimental evidence is offered to support the formation of a ribal intermediate. Since water is associated with many glycosidic bond cleavage pathways and is present in the active site of many enzymes, we subsequently considered direct hydrolysis of the glycosidic bond in dTg. Two reaction pathways (S_N1 and S_N2) were characterized. Both hydrolysis processes are also concerned with significant activation energies. In addition, the effect of water solvent on the reaction profile was evaluated by the CPCM model. All transition states were stabilized by solvent water. The presence of the solvent water substantially lowers all energy barriers.

In summary, both the unimolecular decomposition and hydrolysis involving a single water molecule as the nucleophile are unlikely and are not favorable to the cleavage of the N-glycosidic bond of dTg. This result emphasizes the important catalytic role of enzymes. Our results will have general implications for many biological processes and provide some useful information for our coming work. Currently, we are considering the enzymatic glycosidic bond cleavage of dTg to investigate the effect of enzymes on the energy profile and mechanism.

Acknowledgment. This project has been supported by the National Natural Science Foundation of China (Grant Nos. 20773089 and 20835003) and the Scientific Research Foundation for the Returned Overseas Chinese Scholars, State Education Ministry (Grant No. 20071108-18-15).

Supporting Information Available: Listings of optimized Cartesian coordinates and energies in hartrees at the BHandHLYP/6-311++ G(d,p) level of theory and tables with comparisons between the theoretical geometry at the BHandHLYP/6-311++G(d,p) level and the crystal structure of deoxythymidine glycol. This material is available free of charge via the Internet at http://pubs.acs.org.

References and Notes

(1) Dizdaroglu, M.; Jaruga, P.; Birincioglu, M.; Rodriguez, H. *Free Radical Biol. Med.* **2002**, *32*, 1102–1115.
(2) Ames, B. N.; Gold, L. S. *Mutat. Res.* **1991**, *250*, 3–16.
(3) Gilchrest, B. A.; Bohr, V. A. *FASEB J.* **1997**, *11*, 322–330.
(4) Wiseman, H.; Halliwell, B. *Biochem. J.* **1996**, *313*, 17–29.
(5) Adelman, R.; Saul, R. L.; Ames, B. N. *Proc. Natl. Acad. Sci. U.S.A.* **1988**, *85*, 2706–2708.
(6) Pfeifer, G. P. *Mutat. Res.* **2000**, *450*, 155–166.
(7) Zuo, S.; Boorstein, R. J.; Teebor, G. W. *Nucleic Acids Res.* **1995**, *23*, 3239–3243.
(8) Adelman, R.; Saul, R. L.; Ames, B. N. *Proc. Natl. Acad. Sci. U.S.A.* **1988**, *85*, 2706–2708.
(9) Cathcart, R.; Schwiers, E.; Saul, R. L.; Ames, B. N. *Proc. Natl. Acad. Sci. U.S.A.* **1984**, *81*, 5633–5637.
(10) Lustig, M. J.; Cadet, J.; Boorstein, R. J.; Teebor, G. W. *Nucleic Acids Res.* **1992**, *20*, 4839–4845.
(11) Vaishnav, Y.; Holwitt, E.; Swenberg, C.; Lee, H.-C.; Kan, L.-S. *J. Biomol. Struct. Dyn.* **1991**, *8*, 935–951.
(12) Kao, J. Y.; Goljer, I.; Phan, T. A.; Bolton, P. H. *J. Biol. Chem.* **1993**, *268*, 17787–17793.
(13) Iwai, S. *Angew. Chem., Int. Ed.* **2000**, *39*, 3874–3876.
(14) Brown, K. L.; Adams, T.; Jasti, V. P.; Basu, A. K.; Stone, M. P. *J. Am. Chem. Soc.* **2008**, *130*, 11701–11710.
(15) Miaskiewicz, K.; Miller, J.; Osman, R. *Int. J. Radiat. Biol.* **1993**, *63*, 677–686.
(16) Basu, A. K.; Loechler, E. L.; Leadon, S. A.; Essigmann, J. M. *Proc. Natl. Acad. Sci. U.S.A.* **1989**, *86*, 7677–7681.
(17) McNulty, J. M.; Jerkovic, B.; Bolton, P. H.; Basu, A. K. *Chem. Res. Toxicol.* **1998**, *11*, 666–673.
(18) Ide, H.; Kow, Y. W.; Wallace, S. S. *Nucleic Acids Res.* **1985**, *13*, 8035–8052.
(19) McNulty, J. M.; Jerkovic, B.; Bolton, P. H.; Basu, A. K. *Chem. Res. Toxicol.* **1998**, *11*, 666–673.
(20) Slupphaug, G.; Kavli, B.; Krokan, H. E. *Mutat. Res.* **2003**, *531*, 231–251.
(21) Cathcart, R.; Schniers, E.; Saul, R. L.; Ames, B. N. *Proc. Natl. Acad. Sci. U.S.A.* **1984**, *81*, 5633–5637.
(22) Weiss, B.; Cunningham, R. P. *J. Bacteriol.* **1985**, *162*, 607–610.
(23) Jiang, D.; Hatahet, Z.; Melamede, R. J.; Kow, Y. W.; Wallace, S. S. *J. Biol. Chem.* **1997**, *272*, 32230–32239.
(24) Roldan-Arjona, T.; Anselmino, C.; Lindahl, T. *Nucleic Acids Res.* **1996**, *24*, 3307–3312.
(25) Hilbert, T. P.; Boorstein, R. J.; Kung, H. C.; Bolton, P. H.; Xing, D.; Cunningham, R. P.; Teebor, G. W. *Biochemistry* **1996**, *35*, 2505–2511.
(26) Hilbert, T. P.; Chaung, W.; Boorstein, R. J.; Cunningham, R. P.; Teebor, G. W. *J. Biol. Chem.* **1997**, *272*, 6733–6740.
(27) Hazra, T. K.; Kow, Y. W.; Hatahet, Z.; Imhoff, B.; Boldogh, I.; Mokkapati, S. K.; Mitra, S.; Izumi, T. *J. Biol. Chem.* **2002**, *277*, 30417–30420.
(28) Yamamoto, R.; Akiyama, M.; Ide, H.; Yamamoto, K.; Matsuyama, S.; Kubo, K. *J. Radiat. Res.* **2008**, *49*, 249–259.
(29) Miller, H.; Fernandes, A. S.; Zaika, E.; Mctigue, M. M.; Torres, M. C.; Wente, M.; Iden, C. R.; Grollman, A. P. *Nucleic Acids Res.* **2004**, *32*, 338–345.
(30) McTigue, M. M.; Rieger, R. A.; Rosenquist, T. A.; Iden, C. R.; de los Santos, C. R. *DNA Repair* **2004**, *3*, 313–322.
(31) Katafuchi, A.; Nakano, T.; Masaoka, A.; Terato, H.; Iwai, S.; Hanaoka, F.; Ide, H. *J. Biol. Chem.* **2004**, *279*, 14464–14471.
(32) Lin, J. J.; Sancar, A. *Biochemistry* **1989**, *28*, 7979–7984.
(33) Reardon, J. T.; Bessho, T.; Kung, H. C.; Bolton, P. H.; Sancar, A. *Proc. Natl. Acad. Sci. U.S.A.* **1997**, *94*, 9463–9468.
(34) Kropachev, K. Y.; Zharkov, D. O.; Grollman, A. P. *Biochemistry* **2006**, *45*, 12039–12049.
(35) Takao, M.; Kanno, S.; Shiromoto, T.; Hasegawa, R.; Ide, H.; Ikeda, S.; Sarker, A. H.; Seki, S.; Xing, J. Z.; Le, X. C.; Weinfeld, M.; Kobayashi, K.; Miyazaki, J.; Muijtjens, M.; Hoeijmakers, J. H.; van der Horst, G.; Yasui, A. *EMBO J.* **2002**, *21*, 3486–3493.
(36) Loverix, S.; Geerlings, P.; McNaughton, M.; Augustyns, K.; Vandemeulebroucke, A.; Steyaert, J.; Versees, W. *J. Biol. Chem.* **2005**, *280*, 14799–14802.
(37) Schyman, P.; Danielsson, J.; Pinak, M.; Laaksonen, A. *J. Phys. Chem. A* **2005**, *109*, 1713–1719.
(38) Loverix, S.; Versees, W.; Steyaert, J.; Geerlings, P. *Int. J. Quantum Chem.* **2005**, *106*, 565–570.
(39) Mendieta, J.; Martin-Santamaria, S.; Priego, E.-M.; Balzarini, J.; Camarasa, M.-J.; Perez-Perez, M.-J.; Gago, F. *Biochemistry* **2004**, *43*, 405–414.
(40) Birck, M. R.; Schramm, V. L. *J. Am. Chem. Soc.* **2004**, *126*, 2447–2453.
(41) Mazumder, D.; Kahn, K.; Bruice, T. C. *J. Am. Chem. Soc.* **2002**, *124*, 8825–8833.
(42) Osakabe, T.; Fujii, Y.; Hata, M.; Tsuda, M.; Neya, S.; Hoshino, T. *Chem-Bio Inf. J.* **2004**, *4*, 73–92.
(43) Schramm, V. L. *Arch. Biochem. Biophys.* **2005**, *433*, 13–26.
(44) Millen, A. L.; Archibald, L. A. B.; Hunter, K. C.; Wetmore, S. D. *J. Phys. Chem. B* **2007**, *111*, 3800–381.
(45) Vandemeulebroucke, A.; Versees, W.; De Vos, S.; Van Holsbeke, E.; Steyaert, J. *Biochemistry* **2003**, *42*, 12902–12908.
(46) Hunt, C.; Gillani, N.; Farone, A.; Rezaei, M.; Kline, P. C. *Biochim. Biophys. Acta* **2005**, *1751*, 140–149.
(47) Manuel, R. C.; Hitomi, K.; Arvai, A. S.; House, P. G.; Kurtz, A. J.; Dodson, M. L.; McCullough, A. K.; Tainer, J. A.; Lloyd, R. S. *J. Biol. Chem.* **2004**, *279*, 46930–46939.
(48) Versees, W.; Steyaert, J. *Curr. Opin. Struct. Biol.* **2003**, *13*, 731–738.
(49) Parikh, S. S.; Walcher, G.; Jones, G. D.; Slupphaug, G.; Krokan, H. E.; Blackburn, G. M.; Tainer, J. A. *Proc. Natl. Acad. Sci. U.S.A.* **2000**, *97*, 5083–5088.
(50) Bates, C.; Kendrick, Z.; McDonald, N.; Kline, P. C. *Phytochemistry* **2006**, *67*, 5–12.

(51) Shivakumar, D. M.; Bruice, T. C. *Biochemistry* **2005**, *44*, 7805–7817.
(52) Jiang, Y. L.; McDowell, L. M.; Poliks, B.; Studelska, D. R.; Cao, C.; Potter, G. S.; Schaefer, J.; Song, F.; Stivers, J. T. *Biochemistry* **2004**, *43*, 15429–15438.
(53) Roday, S.; Amukele, T.; Evans, G. B.; Tyler, P. C.; Furneaux, R. H.; Schramm, V. L. *Biochemistry* **2004**, *43*, 4923–4933.
(54) Beck, A. D. *J. Chem. Phys.* **1993**, *98*, 5648–5652.
(55) Parr, R. G.; Yang, W. *Density-Functional Theory of Atoms and Molecules*; Oxford University Press: Oxford, U.K., 1989.
(56) Zhang, Q.; Bell, R.; Truong, T. N. *J. Phys. Chem.* **1995**, *99*, 592–600.
(57) Gonzalez, C.; Schlegel, H. B. *J. Chem. Phys.* **1989**, *90*, 2154–2161.
(58) Reed, A. E.; Weinstock, R. B.; Weinhold, F. *J. Chem. Phys.* **1985**, *83*, 735–746.
(59) Reed, A. E.; Curtiss, L. A.; Weinhold, F. *Chem. Rev.* **1988**, *88*, 899–926.
(60) Barone, V.; Cossi, M. *J. Phys. Chem. A* **1998**, *102*, 1995–2001.
(61) Cossi, M.; Rega, N.; Scalmani, G.; Barone, V. *J. Comput. Chem.* **2003**, *24*, 669–681.
(62) Frisch, M. J.; Trucks, G. W.; Schlegel, H. B.; Scuseria, G. E.; Robb, M. A.; Cheeseman, J. R.; Zakrzewski, V. G.; Montgomery, J. A., Jr.; Stratmann, R. E.; Burant, J. C.; Dapprich, S.; Millam, J. M.; Daniels, A. D.; Kudin, K. N.; Strain, M. C.; Farkas, O.; Tomasi, J.; Barone, V.; Cossi, M.; Cammi, R.; Mennucci, B.; Pomelli, C.; Adamo, C.; Clifford, S.; Ochterski, J.; Petersson, G. A.; Ayala, P. Y.; Cui, Q.; Morokuma, K.; Malick, D. K.; Rabuck, A. D.; Raghavachari, K.; Foresman, J. B.; Cioslowski, J.; Ortiz, J. V.; Stefanov, B. B.; Liu, G.; Liashenko, A.; Piskorz, P.; Komaromi, I.; Gomperts, R.; Martin, R. L.; Fox, D. J.; Keith, T.; Al-Laham, M. A.; Peng, C. Y.; Nanayakkara, A.; Gonzalez, C.; Challacombe, M.; Gill, P. M. W.; Johnson, B.; Chen, W.; Wong, M. W.; Andres, J. L.; Gonzalez, C.; Head-Gordon, M.; Replogle, E. S.; Pople, J. A. *Gaussian 03*, revision D.01; Gaussian, Inc.: Pittsburgh, PA, 2005.
(63) Durant, J. L. *Chem. Phys. Lett.* **1996**, *256*, 595–602.
(64) Csontos, J.; Palermo, N.; Murphy, R.; Lovas, S. *J. Comput. Chem.* **2008**, *29*, 1344–1352.
(65) Yu, W. B.; Liang, L.; Lin, Z. J.; Ling, S. L.; Haranczyk, M.; Gutowski, M. *J. Comput. Chem.* **2008**, *30*, 589–600.
(66) Gelbin, A.; Schneider, B.; Clowney, L.; Hsieh, S. H.; Olson, W. K.; Berman, H. M. *J. Am. Chem. Soc.* **1996**, *118*, 519–529.
(67) Hruska, F. E.; Sebastian, R.; Grand, A.; Voituriez, L.; Cadet, J. *Can. J. Chem.* **1987**, *65*, 2618.
(68) Flippen, J. L. *Acta Crystallogr.* **1973**, *B29*, 1756–1762.
(69) Miaskiewicz, K.; Miller, J.; Osman, R. *Int. J. Radiat. Biol.* **1993**, *63*, 677–686.
(70) Canduri, F.; dos Santos, D. M.; Silva, R. G.; Mendes, M. A.; Basso, L. A.; Palma, M. S.; de Azevedo, W. F.; Santos, D. S. *Biochem. Biophys. Res. Commun.* **2004**, *313*, 907–914.
(71) Moyano, A.; Pericàs, M. A.; Valentí, A. *J. Org. Chem.* **1989**, *54*, 573–582.

JP903334J